Title

Structure of the Bacillus anthracis Sortase A Enzyme Bound to Its Sorting Signal A FLEXIBLE AMINO-TERMINAL APPENDAGE MODULATES SUBSTRATE ACCESS*

Journal

Journal of Biological Chemistry, 290(42)

ISSN

0021-9258

Authors

Chan, Albert H
Yi, Sung Wook
Terwilliger, Austen L
et al.

Publication Date

2015-10-01

DOI

10.1074/jbc.m115.670984

Peer reviewed

THE JOURNAL OF BIOLOGICAL CHEMISTRY VOL. 290, NO. 42, pp. 25461–25474, October 16, 2015

Structure of the *Bacillus anthracis* Sortase A Enzyme Bound to Its Sorting Signal

A FLEXIBLE AMINO-TERMINAL APPENDAGE MODULATES SUBSTRATE ACCESS[*][S]

Received for publication, June 8, 2015, and in revised form, August 5, 2015 Published, JBC Papers in Press, August 31, 2015, DOI 10.1074/jbc.M115.670984

Albert H. Chan[‡§¶], **Sung Wook Yi**[‡], **Austen L. Terwilliger**[‖], **Anthony W. Maresso**[‖], **Michael E. Jung**[‡], **and Robert T. Clubb**[‡§¶1]

From the [‡]*Department of Chemistry and Biochemistry,* [§]*UCLA-DOE Institute of Genomics and Proteomics, and the* [¶]*Molecular Biology Institute, University of California, Los Angeles, California 90095 and the* [‖]*Department of Molecular Virology and Microbiology, Baylor College of Medicine, Houston, Texas 77030*

Background: The *Bacillus anthracis* sortase A ([Ba]SrtA) enzyme attaches virulence factors to the cell surface.
Results: The structure of [Ba]SrtA bound to a substrate analog reveals key amino acids involved in substrate recognition and catalysis.
Conclusion: [Ba]SrtA modulates substrate access using a unique N-terminal appendage.
Significance: This research could facilitate the design of new anti-infective agents that work by disrupting surface protein display.

The endospore forming bacterium *Bacillus anthracis* causes lethal anthrax disease in humans and animals. The ability of this pathogen to replicate within macrophages is dependent upon the display of bacterial surface proteins attached to the cell wall by the *B. anthracis* Sortase A ([Ba]SrtA) enzyme. Previously, we discovered that the class A [Ba]SrtA sortase contains a unique N-terminal appendage that wraps around the body of the protein to contact the active site of the enzyme. To gain insight into its function, we determined the NMR structure of [Ba]SrtA bound to a LP*X*TG sorting signal analog. The structure, combined with dynamics, kinetics, and whole cell protein display data suggest that the N terminus modulates substrate access to the enzyme. We propose that it may increase the efficiency of protein display by reducing the unproductive hydrolytic cleavage of enzyme-protein covalent intermediates that form during the cell wall anchoring reaction. Notably, a key active site loop (β7/β8 loop) undergoes a disordered to ordered transition upon binding the sorting signal, potentially facilitating recognition of lipid II.

Bacillus anthracis is a Gram-positive endospore forming bacterium that causes lethal anthrax disease in humans and animals. Bacterial spores are an infectious form of the pathogen, and predominantly enter the human body through inhalation, ingestion, or cuts in the skin (1). Gastrointestinal (ingestion) and pulmonary (inhalation) forms of anthrax are often fatal if the illness progresses to the fulminant phase (2). In pulmonary anthrax, inhaled spores are first phagocytized by alveolar macrophages in the lungs, and then transported to the lymph nodes. The spores are resistant to killing and germinate into vegetative cells that enter the bloodstream to cause host damage via secreted toxins. The ability of the microbe to thrive and replicate within macrophages is dependent upon the display of bacterial surface proteins that are attached to the cell wall by the *B. anthracis* Sortase A ([Ba]SrtA)[2] enzyme (3). Understanding the mechanism through which this enzyme displays surface proteins is of fundamental importance and could facilitate the design of new anti-infective agents that work by disrupting surface protein display.

[Ba]SrtA is a member of the sortase superfamily, a large group of extracellular membrane-associated cysteine transpeptidase enzymes that are predominantly found in Gram-positive bacteria (4–11). At present, over 800 genes encoding sortase proteins, and a much larger number of sortase protein substrates have been identified in ~260 species of bacteria (12). The sortase A enzyme from *Saccharomyces aureus* ([Sa]SrtA) has been studied in detail. It attaches proteins to the cell envelop by catalyzing a transpeptidation reaction that joins a C-terminal cell wall sorting signal within its protein substrate to the cross-bridge peptide. In this process, a full-length precursor protein containing an amino-terminal leader peptide is exported from the cytoplasm through the secretory (Sec) pathway. The cell wall sorting signal in sortase substrates consists of a LP*X*TG-motif (where *X* denotes any amino acid), followed by a segment of hydrophobic amino acids, and a tail composed primarily of positively charged residues. The C-terminal charged tail presumably retards export, positioning the protein for processing

* This work was supported, in whole or in part, by National Institutes of Health Grants AI52217 (to R. T. C. and M. E. J.), AI097167 and AI109465 (to A. W. M.), and T32 GM008496 (to A. H. C.) and Department of Energy Grant DE-FC-03-87ER60615. The authors declare that they have no conflicts of interest with the contents of this article.
The atomic coordinates and structure factors (code 2RUI) have been deposited in the Protein Data Bank (http://wwpdb.org/).
Chemical shift data have been deposited in the Biological Magnetic Resonance Data Bank under accession code 11570.
[S] This article contains supplemental Tables S1–S3.
[1] To whom correspondence should be addressed: Dept. of Chemistry and Biochemistry, University of California, Los Angeles, 602 Boyer Hall, Los Angeles, CA 90095. Tel.: 310-206-2334; Fax: 310-206-4749; E-mail: rclubb@mbi.ucla.edu.

[2] The abbreviations used are: SrtA, sortase A; SrtB, sortase B; [Ba]SrtA, *B. anthracis* sortase A; [Sa]SrtA, *S. aureus* sortase A; [Sa]SrtB, *S. aureus* sortase B; DAP, *meso*-diaminopimelic acid; HSQC, heteronuclear single quantum coherence; RCI, random coil index; r.m.s., root mean square; Boc, *tert*-butyloxycarbonyl; DNP, 2,4-dinitrophenol.

by the extracellular membrane-associated ^{Sa}SrtA (13). Catalysis occurs through a ping-pong mechanism that is initiated when the active site cysteine residue in ^{Sa}SrtA nucleophilically attacks the backbone carbonyl carbon of the threonine residue within the LP*X*TG motif, breaking the threonine-glycine peptide bond to create a sortase-protein complex in which the components are linked via a thioacyl bond (14, 15). The protein is then transferred by ^{Sa}SrtA to the cell wall precursor lipid II, when the amino group in this molecule nucleophilically attacks the thioacyl linkage to create a peptide bond-linked protein-lipid II product. Transglycosylation and transpeptidation reactions that synthesize the cell wall then incorporate this product into the peptidoglycan. Other members of the sortase superfamily are believed to operate through a similar enzymatic mechanism as ^{Sa}SrtA, but in some microbes (primarily enterococal and corynebacterial species), sortases perform equivalent transpeptidation reactions that assemble pili on the bacterial cell surface (16).

Based on their primary sequences members of the sortase superfamily can be partitioned into at least six subfamilies, called class A to F enzymes (6, 17, 18). The genome of *B. anthracis* encodes class A, B, and D sortases, known as ^{Ba}SrtA, ^{Ba}SrtB, and ^{Ba}SrtC, respectively (19). ^{Ba}SrtA, the focus of this study, anchors seven proteins to the cell wall by joining the threonine of the LP*X*TG sorting signal at the C terminus of the protein to the amine group of *meso*-diaminopimelic acid (DAP) within lipid II (20). ^{Ba}SrtB anchors only one protein to the cell wall, IsdC, which is important for heme binding (21), whereas ^{Ba}SrtC attaches two proteins involved in sporulation (BasH and BasI) (22).

Atomic structures of class A to D enzymes have now been determined revealing a common eight-stranded β-barrel-fold that contains conserved arginine, cysteine, and histidine active site residues (4–11). However, it is not well understood how sortases recognize their sorting signal and nucleophile substrates, because nearly all sortase structures reported to date have been determined in the apo-state. Previously we discovered that the class A ^{Ba}SrtA sortase contains a unique N-terminal appendage that wraps around the body of the protein to contact the active site of the enzyme (23). However, the function of this appendage in catalysis remained unknown. In this article, we report the NMR structure of ^{Ba}SrtA bound to a LP*X*TG sorting signal analog that reveals for the first time the mechanism of substrate recognition by this enzyme. In the structure of the complex, the appendage partially encapsulates the bound sorting signal and we show that these interactions play a role in the *in vivo* and *in vitro* function of the enzyme. A model of the thioacyl intermediate constructed from the coordinates of the complex suggests that the N-terminal appendage may obstruct nucleophile access to the active site. We propose that on the cell surface, the N-terminal appendage may increase the efficiency of protein display by reducing the unproductive hydrolytic cleavage of enzyme-protein covalent intermediates that form during the cell wall anchoring reaction.

Experimental Procedures

Sample Preparation and NMR Spectroscopy—Wild-type SrtA protein from *B. anthracis* containing amino acid residues Asp^{57}-Lys^{210} (^{Ba}SrtA) was produced as described previously (23). Uniformly ^{15}N- and ^{13}C-labeled ^{Ba}SrtA protein was covalently attached to an analog of the LP*X*TG sorting signal, Boc-LPAT* (where T* is (2*R*,3*S*)-3-amino-4-mercapto-2-butanol, and Boc is a *tert*-butyloxycarbonyl protecting group), by incubating 200 μM ^{Ba}SrtA with 2 mM Boc-LPAT* in modification buffer (50 mM Tris-HCl, pH 8.0, 100 mM NaCl) for 48 h at room temperature. MALDI-TOF mass spectrometry was used to confirm the production of stable covalent complex. Two samples of the complex dissolved in NMR buffer (50 mM $NaPO_4$, pH 6.0, 0.01% NaN_3) were studied by NMR: 1) 2.6 mM [^{15}N,^{13}C]^{Ba}SrtA bound to the unlabeled peptide dissolved in NMR buffer containing 8% D_2O; and 2) 2.6 mM [^{15}N,^{13}C]^{Ba}SrtA bound to the unlabeled peptide dissolved in deuterated NMR buffer.

NMR spectra were acquired at 298 K on Bruker Avance 500-, 600-, and 800-MHz spectrometers equipped with triple resonance cryogenic probes. NMR data were processed using NMRPipe (24) and analyzed using PIPP (25) and CARA (version 1.8.4) (26). ^{1}H, ^{13}C, and ^{15}N protein chemical shift assignments were obtained by analyzing the following experiments: ^{15}N-HSQC, ^{13}C-HSQC, HNCACB, CBCA(CO)NH, HNCO, HN(CA)CO, HBHA(CO)NH, HNHA, HNHB, CC(CO)NH, H(CC)(CO)NH, HCCH-TOCSY, and HCCH-COSY (27, 28). Chemical shift assignments of the unlabeled Boc-LPAT* were obtained by analyzing a two-dimensional (F1,F2) ^{13}C-filtered NOESY spectrum (29). Chemical shift data have been deposited in the Biological Magnetic Resonance Data Bank (accession code 11570).

Structure Determination—Distance restraints to define the structure of the protein were obtained from three-dimensional ^{15}N- and ^{13}C-edited NOESY spectra (mixing time at 120 ms), and intermolecular distance restraints between ^{Ba}SrtA and Boc-LPAT* were identified in three-dimensional (F1) ^{13}C,^{15}N-filtered (F2) ^{13}C-edited NOESY-HSQC and (F1) ^{13}C,^{15}N-filtered (F2) ^{15}N-edited NOESY-HSQC (30), and two-dimensional (F1) ^{13}C-filtered NOESY spectra (29). The majority of φ and ψ dihedral angle restraints were obtained using the program TALOS (31). Additional φ angle restraints were obtained by measuring $^{3}J_{HN\alpha}$ values from HNHA spectrum (32), and additional ψ angle restraints were obtained by analyzing three-dimensional ^{15}N-edited NOESY spectrum (33). χ1 angles for dihedral angle restraints and stereotypical chemical shift assignments of β-methylene protons were obtained by analyzing ^{15}N-TOCSY-HSQC, HNHB, HN(CO)HB, and ^{15}N-ROESY spectra (34, 35).

NOE assignments were obtained automatically using the ATNOS and CANDID algorithms in UNIO'10 (36, 37), and structure calculations were performed using XPLOR-NIH (38). The three-dimensional ^{15}N-edited NOESY-HSQC spectrum of the complex dissolved in H_2O, and three-dimensional ^{13}C-edited NOESY-HSQC spectrum of the complex dissolved in D_2O were used as input for UNIO'10. These data were supplemented with dihedral angle restraints and carbon chemical shifts for secondary structure predictions. Seven cycles of ATNOS/CANDID and XPLOR-NIH calculations yielded a converged ensemble of the protein in the complex. All of the NOE assignments made by CANDID were subsequently veri-

fied by manually inspecting the NOESY data. In the structure refinement process, additional intra- and intermolecular distance restraints were identified manually, $^{3}J_{HN\alpha}$ couplings and hydrogen bond restraints were included in structure calculations. Intermolecular NOEs were assigned in an iterative manner. Initially, the positioning of the peptide in the active site was determined using only unambiguous NOEs (intermolecular NOEs that could be readily identified in the filtered and edited NMR spectra of the complex because they were not overlapped with intramolecular protein NOEs). The initial model of the complex was then was used to guide the assignment of more ambiguous intermolecular NOEs. In all cases, only NOEs present in both the filtered and edited NOESY spectra were employed as distance restraints. Hydrogen bonds were identified by inspecting the NOESY data for characteristic patterns along with deuterium exchange experiments, and restraints for hydrogen bonds were implemented with the HBDB algorithm (39). At the final refinement stage, $^{1}D_{NH}$ and $^{1}D_{NCO}$ residual dipolar couplings were included, which were measured using protein samples partially aligned in PEG C12E5/hexanol (40), using two-dimensional ^{15}N-coupled IPAP ^{1}H-^{15}N HSQC and two-dimensional carbonyl-coupled ^{1}H-^{15}N HSQC experiments, respectively (41, 42). Axial and rhombic components of the alignment tensor were fitted using Module (43). In the final set of calculations, a total of 200 structures were generated, of which 94 had no NOE, dihedral angle, or scalar coupling violations greater than 0.5 Å, 5°, or 2 Hz, respectively. Of these, 20 structures with the lowest overall energy were chosen to represent the structure of ^{Ba}SrtA-LPAT* and have been deposited in the Protein Data Bank (PDB code 2RUI). The programs MOLMOL (44) and PyMOL (45) were used to generate figures.

Backbone Dynamics of the ^{Ba}SrtA-LPAT Complex Determined from ^{15}N Relaxation Data*—The ^{15}N relaxation data were collected using a diluted (1.2 mM) ^{15}N- and ^{13}C- labeled sample of the complex dissolved in H_2O on a Bruker Avance 600-MHz NMR spectrometer equipped with a triple resonance cryogenic probe. Data were analyzed using SPARKY (46) and included: ^{15}N longitudinal relaxation rates (R_1), transverse relaxation rates (R_2), and {^{1}H}-^{15}N heteronuclear NOEs. Complete quantifiable relaxation information (R_1, R_2, and NOE) could be measured for 119 of 151 backbone amides. The average R_1, R_2, and NOE values for the complex are 1.47 ± 0.16, 13.14 ± 3.97, and 0.71 ± 0.25 s^{-1}, respectively. The relaxation data were analyzed using the suite of analysis programs kindly provided by Prof. Arthur G. Palmer III, and the strategy used to analyze the relaxation data has been described previously (47). Briefly, Pdbinertia was used to calculate the principal moments of inertia and yielded relative moments of 1.00:0.91:0.68. R2R1_tm was used to calculate an approximate correlation time of 9.3 ± 0.4 ns for rigid residues using R_2/R_1 ratios. To ensure only rigid residues were used in the correlation time analysis, only R_2/R_1 ratios that met the following criteria were used in the analysis: 1) the residue had a {^{1}H}-^{15}N NOE value >0.65, and 2) they were within 1 S.D. of the average. The tensor parameters were then calculated using Quadric_Diffusion (48, 49), which indicated that the isotropic model is statistically preferred for the complex over the axially symmetric or anisotropic models of tumbling. The relaxation data were then interpreted using the Lipari-Szabo Model-free formalism (50, 51) using the program FAST-Modelfree (52) to iteratively run the program Modelfree 4.20 (53). Of the 119 amino acids that gave complete quantifiable relaxation information, data from 98 residues could be fit satisfactorily. Forty-five residues were fit to Model 1 (S^2 only), 3 residues were fit to Model 2 (S^2 and τ_e), 29 residues were fit to Model 3 (S^2 and R_{ex}), 5 residues were fit to Model 4 (S^2, τ_e, and R_{ex}), and 16 residues were fit to Model 5 (S_f^2, S_2^s, and τ_e). S^2 parameters could be measured for backbone amides within all regions of the protein, with the exception of residues in the loop that connects helix H1 and strand β1 (residues 70–79), and the latter half of the β7/β8 loop (residues 192–195).

Modeling of the Thioacyl Intermediate—The procedure used to generate the energy minimized model of the thioacyl intermediate has been described previously (54). Briefly, the methylene group and sulfur of the modified threonine were removed in PyMOL (45), and a carbonyl group was placed between the Cα of the threonine and the sulfur of Cys^{187}, with the oxygen on the carbonyl pointed toward or away from Arg^{196}. The rough models of the thioacyl intermediate were solvated in a periodic water box with a solvent distance of 10 Å, and parameterized in tLEAP (55). Restraints were placed on the initial atom positions of heavy atoms within the protein and the LPAT peptide, except for the side chain atoms of Arg^{196}. Restraints were not placed on the initial coordinates of Arg^{196} because the position of its side chain was not well defined in the ensemble due to peak broadening. Models were then energy minimized and equilibrated in NAMD (56) by slowly removing restraints over 1 ns using 2-fs steps. Details about NAMD set up can be found in Jacobitz *et al.* (54). In the ensemble of NMR structures of the ^{Ba}SrtA-LPAT* complex, the side chain of Arg^{196} adopts multiple conformations and in some conformers its side chain points away from the bound peptide. Importantly, the starting conformation of the arginine side chain prior to energy minimization does not affect its positioning in the model of the thioacyl intermediate, because when test calculations were performed using different starting structures in which the side chain pointed either away or toward the substrate similar results were obtained. Starting models in which the orientation of the oxygen atom within the thioacyl bond pointed toward, or away from, the active site arginine residue (Arg^{196}) also yielded a similar final model of the intermediate after energy minimization.

Site-directed Mutagenesis and Enzyme Kinetics Measurements—Three single amino acid mutants (S59G, I61A, and C187A) of ^{Ba}SrtA were produced for kinetic measurements. Mutations were made using the QuikChange® method (Agilent, San Diego, CA) and confirmed by DNA sequencing. Mutants, wild-type ^{Ba}SrtA (amino acid residues Asp^{57}-Lys^{210}), and wild-type ^{Ba}SrtA$_{\Delta 64}$ (amino acid residues Asp^{65}-Lys^{210}) were purified as described previously (23). *In vitro* substrate hydrolysis assay was performed as previously described (57). Briefly, the cleavage of a self-quenched fluorescent peptide, Abz-LPETG-Dap(Dnp)-NH_2 (Peptide 2.0 Inc., Chantilly, VA), was monitored by excitation at 335 nm and recording emission at 420 nm on an Infinite® M1000 PRO spectrofluorometer (Tecan, San Jose, CA). Assay conditions consisted of 20 mM

HEPES, pH 7.5, and 10 μM enzyme. Abz-LPETG-Dap(Dnp)-NH_2 concentrations between 5 and 320 μM were added to the reaction for a total reaction volume of 50 μl. Fluorescence was recorded for 12 h at 10-min intervals. Initial velocities were calculated in terms of relative fluorescence units/s. Standard curves were used to account for inner filter effects and convert relative fluorescence units to product concentration (14). K_m and k_{cat} values were calculated by direct nonlinear fitting three independent sets of data to the Michaelis-Menten equation using SigmaPlot 6.0 (SPSS, Chicago, IL).

Cellular SrtA Activity Measured by $BasC_{FLAG/MH6}$ Display—pAHG322 plasmids (20) with *$basC_{FLAG/MH6}$* and the WT, S59G, or I61A mutant *srtA* gene were transformed into the *B. anthracis* AHG188 strain (20) lacking *srtA* and transformants selected by plating on LB-chloramphenicol (10 μg/ml). $BasC_{FLAG/MH6}$ was collected by growing 200 ml of each isolate to A_{600} of 1 in LB (AHG188) or LB-chloramphenicol (10 μg/ml, complemented strains). Cells were harvested by centrifugation and resuspended in 5 ml of TSM-lysozyme buffer (50 mM Tris-HCl, pH 7.5, 0.5 M glucose, 10 mM $MgCl_2$, 10 mg/ml of lysozyme), shaken at 37 °C for 4 h, then sedimented by centrifugation at 15,000 $\times$ *g* for 30 min. Purification of $BasC_{FLAG/MH6}$ was achieved by applying cleared lysates to 1 ml of Ni-Sepharose (GE Healthcare, Pittsburgh, PA) and eluting with imidazole as described in Gaspar *et al.* (20). Eluted proteins were precipitated with acetone, subjected to SDS-PAGE, and transferred to a polyvinylidene difluoride membrane. $BasC_{FLAG/MH6}$ was detected by chemiluminescence using an anti-FLAG polyclonal rabbit antibody (F7425, Sigma) and an anti-rabbit HRP secondary antibody (A0545, Sigma). Immunoblot images were quantified by measuring integrated densities of the BasC bands in ImageJ. Normalized values for each biological replicate were used for statistical analysis, and significance determined by a two-tailed Student's *t* test.

Results

Structure of the B. anthracis SrtA Enzyme Bound to a Substrate Analog—To investigate how the *B. anthracis* SrtA sortase recognizes its cognate LP*X*TG sorting signal, we synthesized a peptide analog of this substrate that covalently modifies the enzyme. This peptide, Boc-LPAT*, contains an N-terminal protecting group *t*-butyloxycarbonyl (Boc) and a modified threonine (T*) that replaces the carbonyl group with -CH_2-SH (Fig. 1*A*). The thiol group on T* promotes the formation of a disulfide bond between the peptide and the active site Cys^{187} of the enzyme to generate a covalent complex that structurally mimics the thioacyl intermediate of catalysis (58–60). In this work, we studied a *B. anthracis* SrtA protein construct containing residues Asp^{57}-Lys^{210} (^{Ba}SrtA). ^{Ba}SrtA contains the catalytic core of the enzyme as well as its N-terminal appendage. The solution structure of the ^{Ba}SrtA-LPAT* complex was determined using multidimensional heteronuclear NMR and simulated annealing methods. A total of 2,689 experimental restraints define the structure, including: 1,802 intra-protein NOE distance, 59 intermolecular NOE protein-peptide distance, 318 dihedral angle, 77 $^3J_{HN\alpha}$ coupling, 282 ^{13}C secondary shift, and 151 residual dipolar coupling restraints. Because the peptide is unlabeled, to generate unambiguous intermolecular

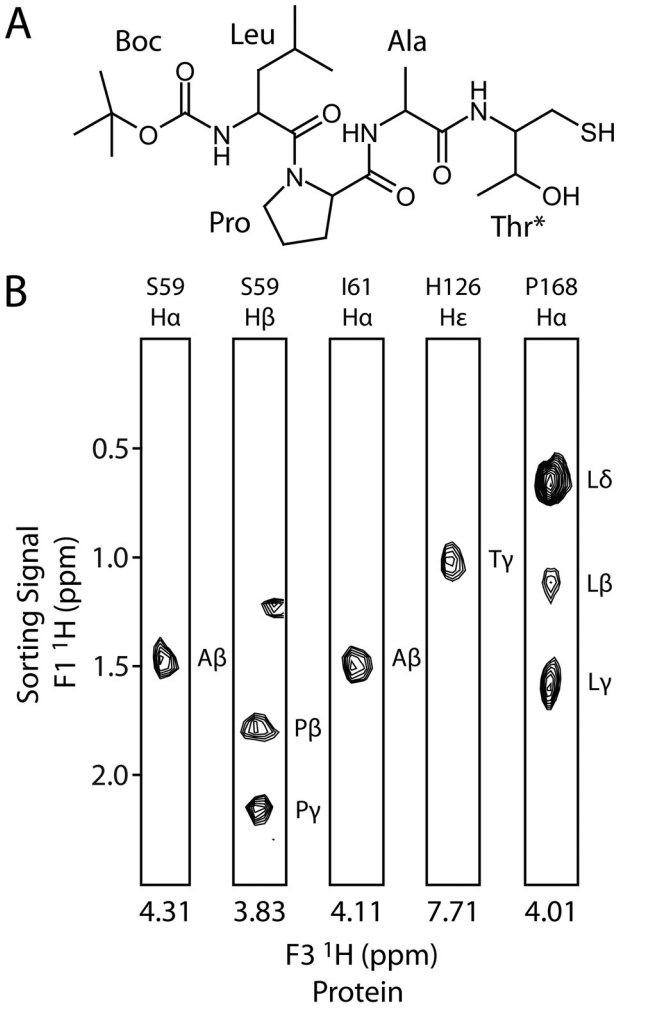

FIGURE 1. **The Boc-LPAT* modifier and NMR data of its complex with ^{Ba}SrtA.** *A,* the chemical structure of the Boc-LPAT* peptide analog, where T* is (2*R*,3*S*)-3-amino-4-mercapto-2-butanol, and Boc is a *tert*-butyloxycarbonyl protecting group. *B,* selected panels showing intermolecular NOEs between ^{Ba}SrtA and the Boc-LPAT* peptide. Panels are taken from a three-dimensional (F1) ^{13}C,^{15}N-filtered, (F2) ^{13}C-edited NOESY-HSQC spectrum of the ^{Ba}SrtA-LPAT* complex dissolved in deuterated buffer. The identity of the proton from ^{Ba}SrtA that gives rise to the set of NOEs and its chemical shift are shown at the *top* and *bottom of each panel*, respectively. On the *right side* of each cross-peak the sorting signal peptide proton that is proximal to the protein is indicated.

NOE protein-peptide distance restraints, we first identified intermolecular NOEs from three-dimensional (F1) ^{13}C,^{15}N-filtered (F2) ^{13}C-edited NOESY-HSQC and three-dimensional (F1) ^{13}C,^{15}N-filtered (F2) ^{15}N-edited NOESY-HSQC spectra, which show only intermolecular NOEs, and then we confirmed the intermolecular NOE assignments with two-dimensional (F1) ^{13}C-filtered NOESY spectrum, which shows both intermolecular and intrapeptide NOEs. An ensemble containing 20 conformers of the structure of the complex is shown in Fig. 2*A*. All conformers possess good covalent geometries and have no NOE, dihedral angle, or scalar coupling violations greater than 0.5 Å, 5°, or 2 Hz, respectively. In the ensemble, backbone atoms of amino acids Asp^{57}-Lys^{210} in the protein, and all residues in the bound peptide are well defined; the backbone and heavy atom coordinate root mean square deviation (r.m.s. deviation) to the average structure are 0.42 $\pm$ 0.06 and 0.89 $\pm$ 0.06 Å,

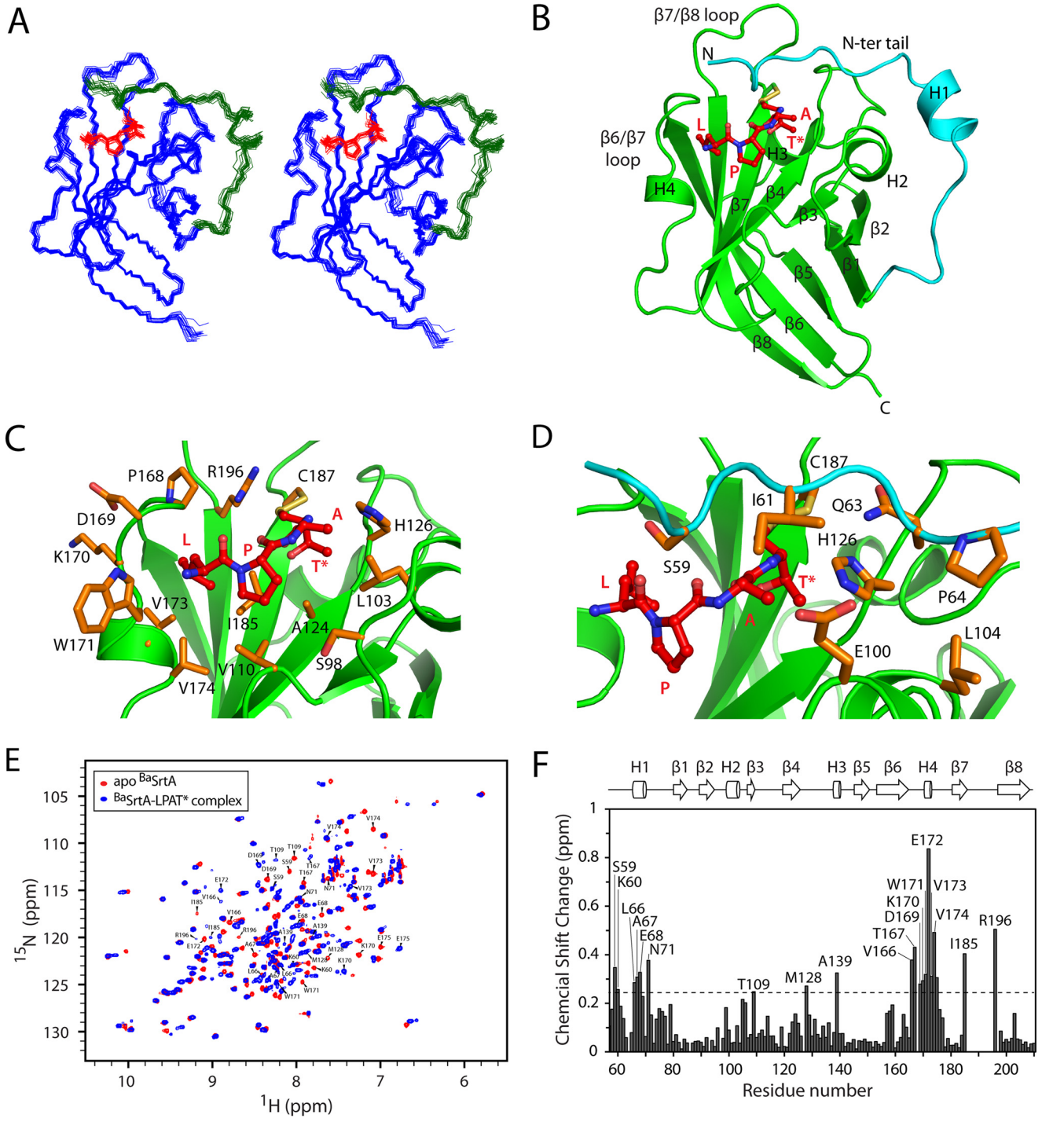

FIGURE 2. **NMR solution structure of the ^{Ba}SrtA-LPAT* complex.** *A,* stereo image showing the ensemble of 20 lowest energy structures of the ^{Ba}SrtA-LPAT complex. The protein backbone heavy atoms (*blue*) and the covalently linked peptide (*red*) are shown. The N-terminal appendage is colored *green*. The coordinates were superimposed by aligning the backbone N, Cα, and C atoms of Asp^{57}-Lys^{210} and Leu, Pro, Ala, and Thr* of the Boc-LPAT* peptide. The backbone and heavy atom coordinates of these residues have a r.m.s. deviation to the average structure of 0.42 and 0.89 Å, respectively. *B,* ribbon drawing of the energy minimized average structure of the ^{Ba}SrtA-LPAT* complex. The covalently bound peptide is shown in a *red* ball-and-stick representation with its amino acids labeled. The N-terminal appendage is colored *cyan*. *C,* expanded view of the active site showing how the sorting signal peptide is recognized. The side chains (*orange*) that participate in the interaction are labeled and shown as sticks. *D,* expanded view of the active site showing how the N-terminal appendage (*cyan*) positions over the sorting signal peptide (*red*). The side chains (*orange*) that participate in the interaction are labeled and shown as sticks. *E,* overlay of the ^{1}H-^{15}N HSQC spectra of apo ^{Ba}SrtA (*red*) and the ^{Ba}SrtA-LPAT* complex (*blue*). *F,* histogram plot of the compound chemical shift changes (Δδ) for the backbone amide hydrogen and nitrogen atoms of apo ^{Ba}SrtA after the addition of Boc-LPAT*. Chemical shift changes are calculated by the equation $\Delta\delta = ((\Delta\delta H)^2 + (\Delta\delta N/6.49)^2)^{1/2}$, where ΔδH and ΔδN are, respectively, the amide proton and nitrogen chemical shift difference for a given residue in the presence and absence of Boc-LPAT*. The *dashed line* represents 1 S.D. above the average Δδ of all amino acids. Amino acids experiencing significant chemical shift changes are labeled, and a schematic of secondary structures of the enzyme is shown *above* the plot.

TABLE 1
Statistics for the NMR structure of ^{Ba}SrtA-LPAT* complex

	$\langle SA \rangle^a$	$\overline{\langle SA \rangle}^a$
R.m.s. deviations from NOE interproton distance restraints (Å)		
All (1861)	0.031 ± 0.002	0.025
Intermolecular (59)	0.054 ± 0.006	0.045
R.m.s. deviations from dihedral angle restraints (degrees)[b] (318)	0.501 ± 0.055	0.970
R.m.s. deviations from $^3J_{HN}{}^{\alpha}$ coupling constant (Hz) (77)	0.701 ± 0.021	0.648
R.m.s. deviations from secondary ^{13}C shifts		
$^{13}C_{\alpha}$ (ppm) (141)	1.166 ± 0.021	1.188
$^{13}C_{\beta}$ (ppm) (141)	1.187 ± 0.021	1.196
Residual dipolar coupling *R*-factors (%)[c]		
D_{NH} (84)	4.3 ± 0.2	6.4
$D_{NC'}$ (67)	23.1 ± 0.8	27.9
Deviations from idealized covalent geometry		
Bonds (Å)	0.0084 ± 0.0001	0.0082
Angles (degrees)	0.748 ± 0.013	0.769
Impropers (degrees)	0.814 ± 0.013	0.872
PROCHECK-NMR[d]		
Most favorable region (%)	88.5 ± 1.2	87.8
Additionally allowed region (%)	10.6 ± 1.3	11.5
Generously allowed region (%)	1.0 ± 0.5	0.7
Disallowed region (%)	0.0 ± 0.0	0.0
Coordinate precision[e]		
Protein backbone (Å)	0.42 ± 0.06	
Protein heavy atoms (Å)	0.89 ± 0.06	

[a] $\langle SA \rangle^a$ represents an ensemble of the 20 best structures calculated by simulated annealing. $\langle SA \rangle^a$ represents the average energy-minimized structure. The number of terms for each restraint is given in parentheses. None of the structures exhibited distance violations greater than 0.5 Å, dihedral angle violations greater than 5°, or coupling constant violations greater than 2 Hz.
[b] Experimental dihedral angle restraints comprised 150 ϕ, 144 ψ, and 24 χ_1 angles.
[c] The dipolar coupling R-factor ranges between 0 and 100% and is defined as the ratio of the r.m.s. deviation between observed and calculated values to the expected r.m.s. deviation if the vectors were randomly distributed, given by $[2D_a^2(4 + 3\eta^2)/5]^{1/2}$, where D_a is the magnitude of the principle component of the alignment tensor, and η is the rhombicity, calculated to be 10.6 Hz and 0.19, respectively.
[d] PROCHECK-NMR data includes residues Asp^{57} to Lys^{210} of ^{Ba}SrtA, and the substrate analog Boc-LPAT*.
[e] The coordinate precision is defined as the average atomic r.m.s. deviation of the 20 individual SA structures and their mean coordinates. The reported values are for residues Asp^{57} to Lys^{210} of ^{Ba}SrtA, and the LPAT* part of the substrate analog. The backbone value refers to the N, C_{α}, and C′ atoms.

respectively. Complete structure and restraint statistics are presented in Table 1.

In the structure of the ^{Ba}SrtA-LPAT* complex, the catalytic core of the enzyme recognizes the LPAT portion of the sorting signal via a large groove that leads into the active site, and the N-terminal appendage that precedes the catalytic core partially shields the peptide from the solvent (Fig. 2*B*). On the catalytic domain, the floor of the LPAT binding groove is formed by residues in strands β4 and β7, and its walls are formed by surface loops that connect strand β6 to β7 (β6/β7 loop), strand β3 to strand β4 (β3/β4 loop), and strand β2 to helix H2 (β2/H2 loop). Within the groove the peptide adopts an "L"-shaped conformation, and it is positioned so as to join the C-terminal end of the signal via a disulfide bond to the active site cysteine residue.

The leucine, proline, and threonine residues within the substrate are recognized by the enzyme. Following convention, residues N-terminal to the Thr-Gly scissile peptide bond in the bound peptide are referred to as P1 to P4, and the corresponding subsites that they interact with on the enzyme are referred to as S1 to S4, respectively (61). The S4 binding site is formed by a pocket created by residues at the N-terminal end of the β6/β7 loop, and strands β6 and β8. The leucyl side chain within the pocket is contacted by the non-polar side chains of Val^{173} and Val^{174} in the 3_{10}-helix H4, as well as by the α-protons of nearby residues in the loop (Pro^{168}, Asp^{169}, Lys^{170}, and Trp^{171}) (Fig. 2*C*). The bottom portion of the S4 pocket is formed by residues Val^{166}, Ile^{185}, and Val^{198}, which together with the β6/β7 loop encapsulate the leucine so as to bury ~90% of the accessible surface area of the side chain. The proline residue forms a ~90° kink, redirecting the trajectory of the peptide toward Cys^{187} within the active site. It is recognized by the S3 site, which is formed by side chains projecting from the floor of the groove (Ala^{124} and Ile^{185} in strands β4 and β7, respectively), and by residues within the surrounding walls (Val^{174}, Val^{110}, and Ser^{98} in β6/β7 loop, β3/β4 loop, and β2/H2 loop, respectively). The proline also makes contacts with the side chain of Ser^{59} within the N-terminal appendage, which is poised to interact with its carbonyl group. The alanine residue in the peptide is located at the *X* position of the LP*X*TG motif. Notably, its side chain methyl does not appear to be recognized as it is positioned on the surface of the enzyme in between Leu^{103} in helix H2 and Ile^{61} in the N-terminal appendage. This surface appears to be large enough to accommodate a range of amino acid side chains, consistent with the documented promiscuity of ^{Ba}SrtA for this site within the sorting signal (62). The side chain of the threonine residue in the substrate is buried in the S1 pocket formed by the side chains of Ile^{185} in strand β7, Ala^{124} in strand β4, and Leu^{103} in helix H2 (Fig. 2, *C* and *D*). The threonine γ-methyl group is also packed underneath the imidazole ring of the active site His^{126} residue. This interaction is substantiated by the intermolecular NOE cross-peaks between the γ-methyl group and the ϵ1- and α-protons of His^{126} (Fig. 1*B*). For a complete list of intermolecular NOEs identified and used in structure calculations, see supplemental Table S1. Extensive chemical shift assignments for apo-^{Ba}SrtA have been reported previously (23) enabling a comparison to the chemical shifts of the ^{Ba}SrtA-LPAT* complex. The chemical shifts of both forms of the protein are presented in supplemental Table S2. Compatible with the structure, the most significant chemical shift changes in the protein that result from peptide binding localize to residues within the binding groove and N-terminal appendage that contact the substrate (Fig. 2, *E* and *F*).

The N-terminal Appendage Partially Encapsulates the Bound Sorting Signal—The catalytic domain of ^{Ba}SrtA is preceded by a structured N-terminal polypeptide segment that is formed by residues Asp^{57}-Val^{79}. The first eight residues, Asp^{57}-Pro^{64}, adopt an extended conformation and partially shield the bound peptide and the active site His^{126} residue from the solvent. The remainder of the N-terminal appendage contains a short helix (H1, residues Leu^{66}-Asn^{71}) and wraps around the surface of the catalytic domain to contact helix H2 and the β2/H2 loop. Two residues in the N-terminal appendage interact with the bound peptide, Ser^{59} and Ile^{61} (Fig. 2*D*). The non-polar side chain of Ile^{61} interacts with the alanine side chain in the bound peptide and it also forms extensive contacts to His^{126} in the active site. An inspection of the ensemble suggests that the hydroxyl group of Ser^{59} is appropriately positioned to donate a hydrogen bond to the backbone carbonyl oxygen of the proline residue in the bound peptide (present in 30% of the conformers). Several intermolecular NOEs position the N-terminal appendage near

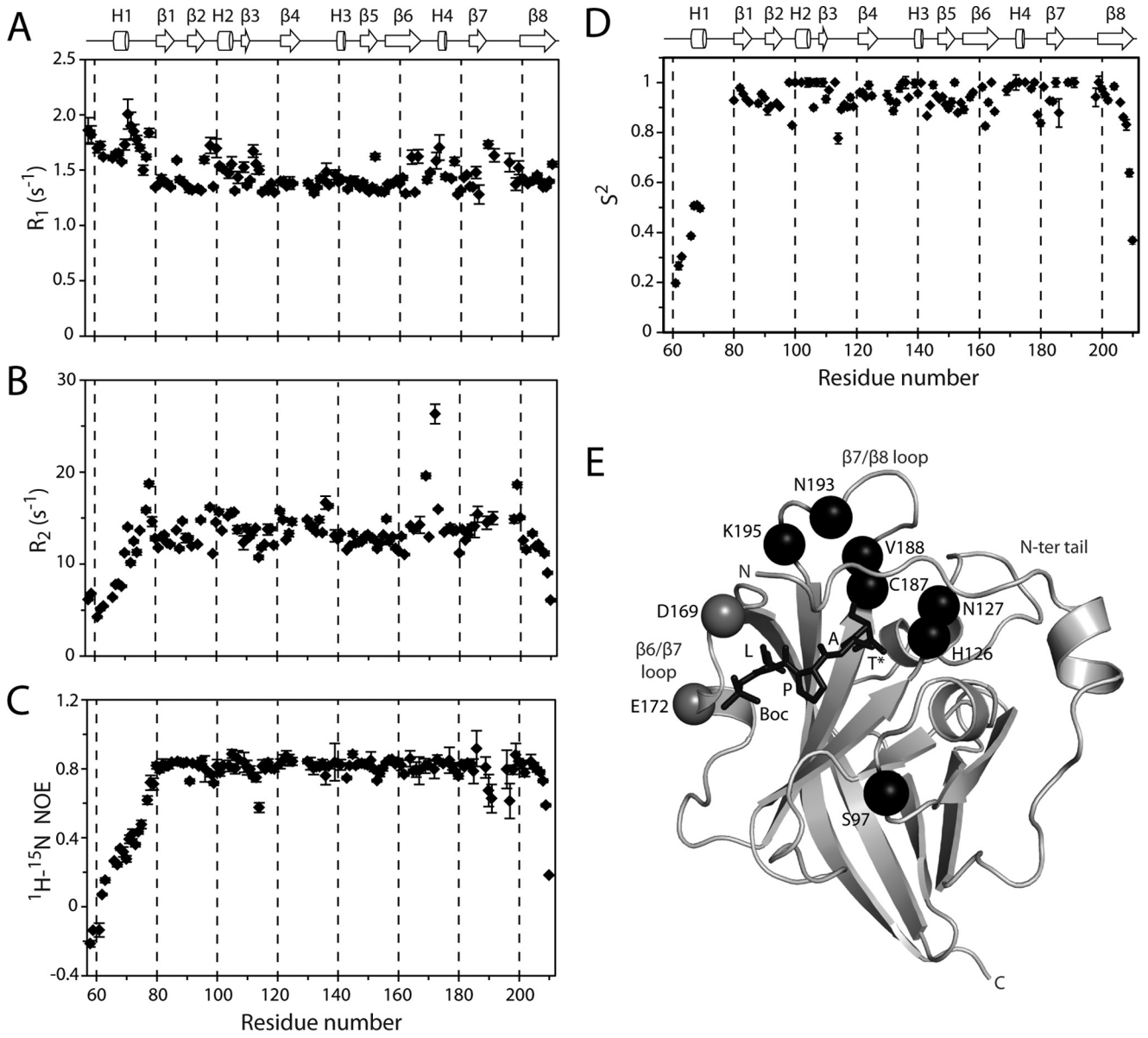

FIGURE 3. **Mobility of ^{Ba}SrtA-LPAT* as defined by NMR relaxation data.** *Panels A–D* are scatter plots of the relaxation data for the complex: R_1 (*A*), R_2 (*B*), ^{1}H-^{15}N heteronuclear NOE (*C*), and general order parameter S^2 of the backbone ^{15}N atoms (*D*) as a function of residue number. The value of S^2 ranges from 0 to 1, with a value of 1 indicating that the amide bond is completely immobilized. The secondary structures present in the protein are displayed on *top* of each plot. *E*, ribbon drawing of ^{Ba}SrtA-LPAT* showing the location of residues in which the backbone amide resonances could not be assigned (*black spheres*), or residues that have R_{ex} values greater than 10 Hz (*gray spheres*).

the peptide. These include NOE cross-peaks between: the α-proton of Ser^{59} and β-methyl group of alanine in the peptide, the β-protons of Ser^{59} and β- and γ-protons of the proline residue in the peptide, and the α-proton of Ile^{61} and β-methyl group of alanine in the peptide (Fig. 1*B*).

^{15}N Relaxation Measurements: the N-terminal Appendage Transiently Detaches from the Enzyme—To investigate backbone motions within the ^{Ba}SrtA-LPAT* complex, we measured the {^{1}H}-^{15}N NOEs, spin-lattice (R_1), and spin-spin (R_2) relaxation rates of the protein backbone nitrogen atoms, and interpreted the data using the Model-free formalism (63). Of the 151 non-proline amino acids in the protein, complete quantifiable relaxation information (NOE, R_1, and R_2) can be obtained for 119 residues, of which data from 98 of these residues could be interpreted using the Model-free approach. This analysis yields three parameters that describe the motion of the protein backbone: the general order parameter S^2, the effective correlation time for internal motion τ_e, and R_{ex}. S^2 reports the backbone mobility of the amide on the picosecond time scale and is characterized by the internal correlation time τ_e. The value of S^2 ranges from 0 to 1, with a value of 1 indicating that the amide bond is completely immobilized. R_{ex} is the chemical exchange contribution to R_2 and is diagnostic for the presence of slower micro- to millisecond time scale motions. The R_1, R_2, ^{1}H-^{15}N NOEs, and S^2 data are shown in Fig. 3, *A–D*. The complete Model-free analysis results are presented as supplemental Table S3). Notably, similar R_2 values are obtained when data are acquired using a more dilute protein sample (180 μM ^{Ba}SrtA-LPAT* complex), indicating that the complex is not aggregating.

The relaxation data indicate that the N-terminal appendage transiently detaches from the enzyme to adopt a disordered state. This is evident from ^{1}H-^{15}N NOE data that shows a gradient of increasing mobility toward the N terminus, presumably because the polypeptide progressively unlatches ("unzips") from the enzyme starting at its N terminus (Fig. 3*C*). Because the Model-free analysis only indirectly reveals the presence of R_{ex} contributions to relaxation, we also performed constant-relaxation time Carr-Purcell-Meiboom-Gill (CPMG) experiments (64) that probe motions occurring on time scales ranging from 0.1 to 10 ms (63, 65, 66). However, analysis of ^{15}N-CPMG relaxation dispersion curves did not reveal the presence of R_{ex} in the N-terminal appendage (data not shown). This indicates that the motions that detach the amino-terminal residues in the appendage from the enzyme occur on a time scale that is faster than 100 μs (66).

In contrast to the N-terminal appendage that partially encapsulates the signal, the peptide binding surface on the catalytic domain adopts a rigid conformation. In particular, both the aforementioned $\beta7/\beta8$ and $\beta6/\beta7$ active site loops are rigid on the picosecond time scale according to their S^2 data (S^2 values for residues in these regions are >0.87). Overall, few residues exhibit significant R_{ex} values in the signal binding pocket. A notable exception are backbone amide atoms of Asp^{169} and Glu^{172} within the $\beta6/\beta7$ loop that are located next to the N-terminal Boc protecting group of the bound peptide that is likely in motion (Fig. 3*E*). In addition, several residues near the active site exhibit resonance line broadening that prevented their chemical shift assignment: Ser^{97} within the $\beta2$/H2 loop, His^{126} and Asn^{127} in the $\beta4/\beta5$ loop, Cys^{187} in the end of strand $\beta7$, and residues Val^{188}, Asn^{193}, and Lys^{195} in the $\beta7/\beta8$ loop. These residues may be broadened as a result of localized protein motions in the active site, binding of the N-terminal appendage and/or changes in the tautomerization state of the imidazole side chain of His^{126}.

The N-terminal Appendage Slows Peptide Hydrolysis and Contributes to Protein Display in Intact Cells—To understand the role of the N-terminal appendage in catalysis, a FRET-based assay was used to monitor the ability of wild-type and mutant ^{Ba}SrtA proteins to hydrolyze a self-quenched fluorescent peptide substrate (Abz-LPETG-Dap(Dnp)-NH_2). Notably, we were unable to reproduce the transpeptidation reaction *in vitro* using diaminopimelic acid as a nucleophile, which is the moiety on lipid II to which surface proteins are attached. This suggests that sortase recognizes additional features on lipid II. The kinetics of hydrolysis were determined for wild-type ^{Ba}SrtA, and three mutants: $^{Ba}SrtA_{\Delta64}$, which removes Asp^{57}-Pro^{64}, and $^{Ba}SrtA_{S59G}$ and $^{Ba}SrtA_{I61A}$ single amino acid mutants that based on the structure should alter interactions between the appendage and the substrate (Fig. 4*A*). Wild-type ^{Ba}SrtA cleaves the peptide with k_{cat} and K_m values of $3.6 \times 10^{-5} \pm 2 \times 10^{-6}$ s^{-1} and 306 ± 23 μM, respectively (Table 2). In contrast, removal of residues Asp^{57}-Pro^{64} ($^{Ba}SrtA_{\Delta64}$) causes a ~60% increase in k_{cat} and ~43% decrease in K_m. Based on the K_m change it seems likely that part of the inhibitory effect of the appendage occurs because its residues collectively obstruct peptide binding to the active site when the isolated enzyme is studied. This is substantiated by data from $^{Ba}SrtA_{S59G}$ and $^{Ba}SrtA_{I61A}$, because these proteins contain mutations that should disrupt appendage-substrate interactions, but they have K_m values similar to the wild-type protein. As described under "Discussion," the finding that the $^{Ba}SrtA_{I61A}$ and $^{Ba}SrtA_{\Delta64}$ mutants have increased k_{cat} values relative to the wild-type protein is compatible with the amino-terminal appendage acting to slow hydrolysis of the thioacyl intermediate.

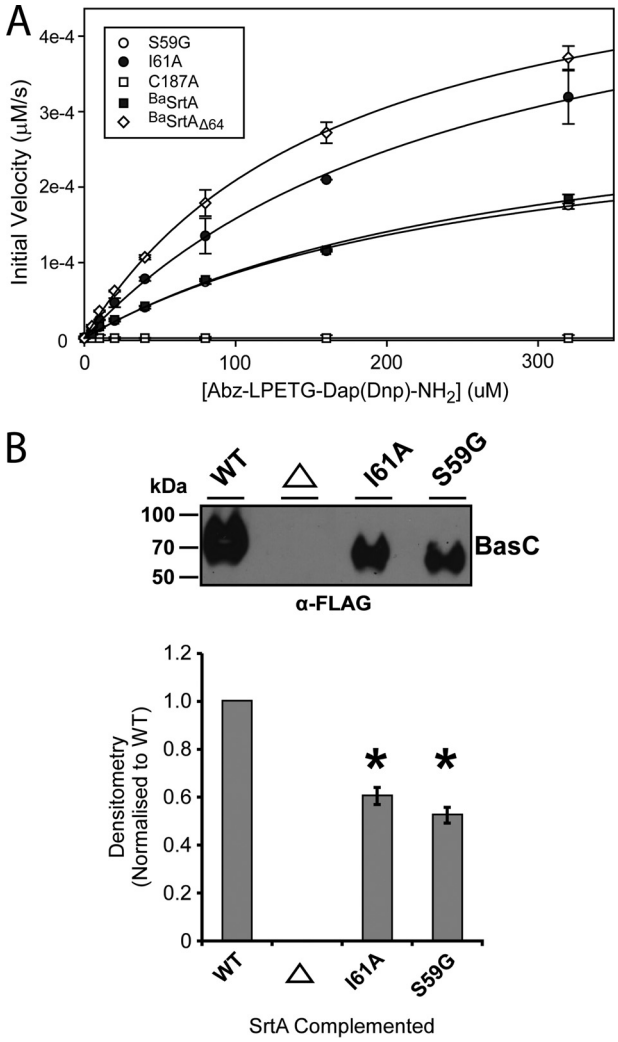

FIGURE 4. **Effects of mutating the N-terminal appendage on enzyme kinetics and protein display in *B. anthracis*.** *A*, representative curves showing the *in vitro* hydrolysis kinetics of S59G (*open circles*), I61A (*filled circles*), and C187A (*open squares*) mutants of ^{Ba}SrtA, as well as the hydrolysis kinetics of wild-type ^{Ba}SrtA (*filled squares*). Also shown is the progress curve for mutant of ^{Ba}SrtA that removes a portion of the N-terminal appendage ($^{Ba}SrtA_{\Delta64}$, identical to ^{Ba}SrtA except residues Asp^{57}-Pro^{64} are absent). *B*, the effects of mutations in the N-terminal appendage of sortase on BasC protein display in *B. anthracis.* Sterne 34F2 strains lacking *srtA* (△) or complemented with the indicated *srtA* and $basC_{FLAG/MH6}$ on pAHG322 were grown to an A_{600} of 1, and the harvested cells digested with lysozyme to liberate $BasC_{FLAG/MH6}$. Cleared lysates were purified via affinity chromatography and the resulting eluates were analyzed for the presence of $BasC_{FLAG/MH6}$ by immunoblotting with anti-FLAG polyclonal antibodies. A representative blot is shown at the *top*. Biological replicates were quantified and normalized to the $BasC_{FLAG/MH6}$ anchored by WT SrtA. Means are plotted with standard error at the *bottom panel*. * = $p < 0.01$, $n = 3$.

To investigate the biological importance of the N-terminal appendage we determined how mutating this segment in ^{Ba}SrtA affected its ability to display proteins in intact *B. anthracis* cells. Protein display was monitored in a Δ*srtA* strain of

TABLE 2
Enzyme hydrolysis kinetics of the ^{Ba}SrtA enzyme

	k_{cat}	K_m	k_{cat}/K_m
	s^{-1}	μM	$\mu M^{-1}s^{-1}$
S59G	$3.3 \times 10^{-5} \pm 1 \times 10^{-6}$	280 ± 16	$1.2 \times 10^{-7} \pm 8 \times 10^{-9}$
I61A	$5.8 \times 10^{-5} \pm 5 \times 10^{-6}$	265 ± 38	$2.2 \times 10^{-7} \pm 4 \times 10^{-8}$
C187A	NA[a]	NA	NA
^{Ba}SrtA	$3.6 \times 10^{-5} \pm 2 \times 10^{-6}$	306 ± 23	$1.2 \times 10^{-7} \pm 1 \times 10^{-8}$
^{Ba}SrtA$_{\Delta 64}$	$5.7 \times 10^{-5} \pm 2 \times 10^{-6}$	173 ± 11	$3.3 \times 10^{-7} \pm 2 \times 10^{-8}$

[a] NA, not active.

B. anthracis (strain AHG188) that was transformed with plasmid (pAHG322) that expresses wild-type or mutated ^{Ba}SrtA, as well as the BasC$_{FLAG/MH6}$ reporter protein. BasC$_{FLAG/MH6}$ has previously been shown to be anchored to the cell wall by sortase and contains the full-length BasC substrate of sortase harboring an active cell wall sorting signal, as well as His$_6$ and FLAG tags that facilitate its fractionation and immunoblot detection, respectively (20). The cell wall of *B. anthracis* was fractionated and BasC$_{FLAG/MH6}$ was detected by immunoblotting with anti-FLAG polyclonal antibodies. Fig. 4*B* shows a representative Western blot, as well as the quantified results from three replicates of the experiment. S59G and I61A mutants of ^{Ba}SrtA decreased the amount of BasC$_{FLAG/MH6}$ found in the cell wall by ~40 and ~50%, respectively, when compared with wild-type ^{Ba}SrtA. Although our results may be complicated by the presence of unprocessed BasC$_{FLAG/MH6}$ trapped in the membrane, a significant decrease in BasC$_{FLAG/MH6}$ present in the cell wall fraction indicates that the N-terminal appendage in ^{Ba}SrtA plays a role in sortase catalyzed attachment of surface proteins in *B. anthracis*.

Discussion

Sortase enzymes are used by Gram-positive bacteria to covalently attach protein virulence factors to the bacterial cell surface and therefore are promising drug targets (6, 67). An understanding of the mechanism of substrate recognition could facilitate the rational development of sortase inhibitors. Previously, we reported the structure of the SrtA enzyme from *B. anthracis* (^{Ba}SrtA) that anchors surface proteins required for bacterial escape from macrophages, a key step in the progression of lethal anthrax disease (3). In contrast to previously studied sortases, ^{Ba}SrtA contains a unique N-terminal polypeptide appendage that directly interacts with its active site histidine residue (His^{126}). However, the function of the appendage and its role in signal recognition remained unclear. Here we report NMR studies that show that the appendage in ^{Ba}SrtA directly contacts the bound sorting signal, potentially increasing the efficiency of sortase-mediated cell wall protein anchoring by retarding the spurious hydrolysis of a key thioacyl reaction intermediate.

^{Ba}SrtA binds its sorting signal via a preformed binding groove located in the catalytic domain, which surprisingly triggers a disordered to ordered transition in the adjacent $\beta7/\beta8$ active site loop. The vast majority of enzyme interactions with the signal are mediated by residues located in a structurally ordered binding groove that is formed by residues in $\beta6/\beta7$ loop (Val^{166}-Val^{174}), strand $\beta4$ (Ala^{124}), strand $\beta7$ (Ile^{185}), $\beta3/\beta4$ loop (Val^{110}), $\beta2$/H2 loop (Ser^{98}), and helix H2 (Leu^{103}) (Fig. 2*A*). In the apo-form of ^{Ba}SrtA, residues in the groove adopt a fixed structure and undergo only small positional changes upon ligand binding (the backbone atoms of the residues in the complex that form the pocket are aligned with an r.m.s. deviation of 0.76 Å to the structure of the apo-form of ^{Ba}SrtA). In contrast to this preordered binding groove, the $\beta7/\beta8$ loop in the active site experiences large changes in its dynamics and structure when the signal binds (Fig. 5*A*). In the apo-form of ^{Ba}SrtA, the $\beta7/\beta8$ loop is structurally disordered and its residues undergo motions on the micro to millisecond time scales; the backbone amide resonances of nearly all of its residues exhibited substantial motion-induced line broadening (only the backbone amide of Lys^{196} could be assigned). In contrast, in the ^{Ba}SrtA-LPAT* complex, the coordinates of the $\beta7/\beta8$ loop become well defined and more immobilized. The substrate dependent disorder-to-order transition is evidenced by the NMR relaxation data, our ability to assign the majority of backbone amide resonances of the loop in the NMR spectra of the complex (only the backbone amides of Val^{188}, Asn^{193}, and Lys^{195} could not be assigned), and by the observation of numerous NOEs in the NOESY spectra that define the structure of the loop. It is also supported by NOESY spectra of the free and bound forms of the protein, because key long range and intra-loop NOE cross-peaks that are present in the spectra of the bound enzyme are either absent or significantly less intense (~6-fold less intense) in the spectra of the apo-form. Collectively, these data strongly suggest that binding of the substrate causes the $\beta7/\beta8$ loop to become more structurally ordered and immobilized.

Interestingly, substrate binding indirectly causes conformational ordering of the $\beta7/\beta8$ loop by displacing the polypeptide backbone containing the active site Cys^{187} residue. In the complex, the peptide forms a covalent bond with the thiol of Cys^{187} located at the end of strand $\beta7$ immediately preceding the $\beta7/\beta8$ loop. Peptide binding causes the backbone atoms Cys^{187} to shift by ~7 Å away from the signal, which in turn displaces the $\beta7/\beta8$ loop (Fig. 5*A*). As a result, the $\beta7/\beta8$ forms stabilizing interactions with residues in the $\beta4/\beta5$ loop; the side chain of Val^{190} within the $\beta7/\beta8$ loop packs against Met^{128} and Ser^{129} within the $\beta4/\beta5$ loop. The structural change in the $\beta7/\beta8$ loop may play an important role in catalysis as this loop has been postulated to form a surface that recognizes the second substrate of catalysis, lipid II (68, 69). This may be a common feature of class A enzymes, as similar positional changes in the $\beta7/\beta8$ loop have been observed in the *S. aureus* SrtA enzyme as a result of substrate binding.

Modeling studies suggest that the appendage may transiently mask the thioacyl intermediate. We modeled the thioacyl enzyme-substrate reaction intermediate using the NMR structure of the ^{Ba}SrtA-LPAT* complex. The coordinates of the methylene group and sulfur atom in the modified threonine residue in the sorting signal were replaced by a carbonyl group, and a thioacyl bond to the active site cysteine was established. The coordinates were then energy minimized to yield a model of the thioacyl reaction intermediate. In test calculations, a range of starting structures were energy minimized in which the active site arginine and carbonyl oxygen were positioned differently. In all cases, these calculations yielded the same basic model shown in Fig. 6 (see "Experimental Procedures" for

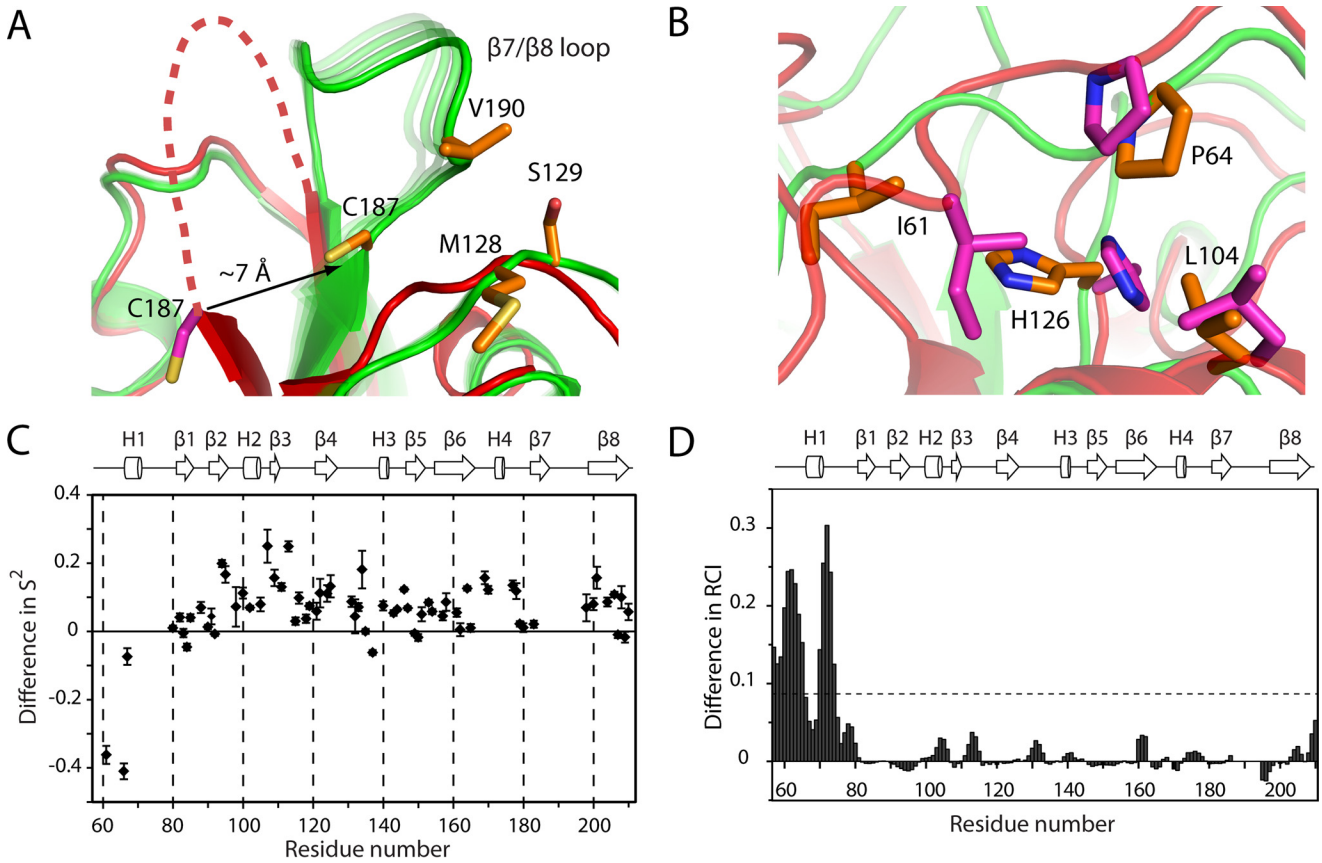

FIGURE 5. **Comparison of the structure of ^{Ba}SrtA in its apo and LPAT* bound states.** *A,* ribbon drawing showing the superposition of the structures of apo ^{Ba}SrtA (PDB code 2KW8; *red*) and the ^{Ba}SrtA-LPAT* complex (*green*). Key residues are represented as *sticks* and colored *orange* (^{Ba}SrtA-LPAT*) or *magenta* (apo ^{Ba}SrtA). An expanded view of the *β*7/*β*8 loop is shown. The loop transitions from a disordered state (represented by *dotted line*) to an ordered state after binding the substrate. Cys^{187} is displaced by ~7 Å away from the substrate binding pocket, facilitating new contacts between the side chains of Val^{190}, Met^{128}, and Ser^{129}. The N-terminal appendage and Boc-LPAT* are removed for clarity. *B,* as in *panel A*, but an expanded view of the N-terminal appendage and its interactions with the active site is shown. Ile^{61} is displaced when the substrate binds such that it only partially buries His^{126}. The backbone atoms of Ile^{61}-Thr^{186} and Arg^{196}-Lys^{210} of the two structures align to a r.m.s. deviation of 0.73 Å. *C,* scatter plot showing the change in the general order parameter S^2 after the addition of Boc-LPAT*. A *positive number* indicates the backbone amide becomes more rigid, whereas a *negative number* indicates it becomes more disordered. A schematic of secondary structures in the enzyme is shown *above* the plot. *D,* histogram plot of the difference in RCI between Boc-LPAT* bound ^{Ba}SrtA and apo ^{Ba}SrtA. The *dashed line* represents 1 S.D. above the average difference in RCI (random coil index) for all amino acids. A positive value indicates that protein likely becomes less structured upon binding the substrate. A schematic of secondary structures of the enzyme is shown *above* the plot.

details). In the model of the thioacyl intermediate, the side chain of Arg^{196} makes extensive contacts with the LPAT peptide. Its side chain is wedged into a pocket that is enclosed by the L-shaped backbone of the peptide, with its guanidino group hydrogen bonding to the backbone carbonyl oxygen of proline, and to the side chain γ-hydroxyl group of the threonine. The latter interaction is compatible with the existence of a substrate-stabilized oxyanion hole as previously postulated for the *S. aureus* SrtB enzyme (54). This is because the oxygen atom presumably moves by only ~0.5 Å during the transition between sp^2 and sp^3 hybridization of the carbonyl carbon atom, such that the cationic guanidino group can be expected to remain near the oxyanion of the tetrahedral for favorable interactions, and to interact with the γ-hydroxyl group of threonine residue within the sorting signal. Notably, the N-terminal appendage in the model of the thioacyl enzyme-substrate reaction intermediate remains positioned over the sorting signal. This shields the electrophilic carbon atom in the thioacyl bond from the solvent, thus the appendage may obstruct the nucleophilic attack of the intermediate by lipid II or water. However, the obstruction is transient in nature and does not completely inhibit the isolated enzyme because the N-terminal residues in the appendage frequently detach from the enzyme based on the NMR relaxation data.

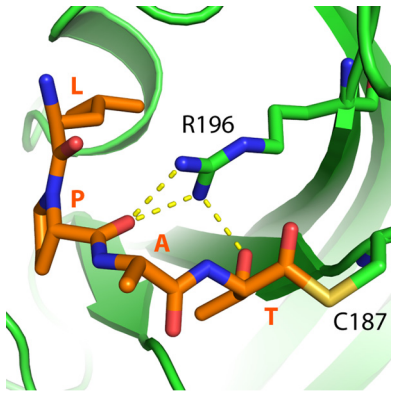

FIGURE 6. **Model of the thioacyl intermediate.** Expanded view of the active site in the energy minimized model of the ^{Ba}SrtA-LPAT thioacyl intermediate. The peptide substrate LPAT (*orange*) and active site residues Cys^{187} and Arg^{196} (*green*) are shown as *sticks*. Hydrogen bonds are indicated by *yellow dotted lines*. The distance between Thr carbonyl oxygen and Arg^{196} guanidino Cζ is 3.6 Å.

In addition to the structure of the ^{Ba}SrtA-LPAT* complex, two structures of sortase enzymes covalently bound to their sorting signal have been reported: the NMR and crystal structures of *S. aureus* SrtA and SrtB enzymes bound to LPAT* and NPQT* substrate analogs, respectively (54, 68). A detailed comparison of these structures with the ^{Ba}SrtA-LPAT* complex is beyond the scope of this article. However, as in the ^{Ba}SrtA-LPAT* complex, the proline in these structures causes the sorting signal to adopt an L-shaped conformation that is critical for positioning of the P4 residue. Moreover, in both the ^{Ba}SrtA-LPAT* and ^{Sa}SrtB-NPQT* structures, the threonine residue in the bound signal points "in" toward the floor of the substrate binding site where it is poised to interact with active site arginine (Arg^{196} and Arg^{233}, in ^{Ba}SrtA and ^{Sa}SrtB, respectively). As described in detail in Jacobitz *et al.* (54) this suggests ^{Ba}SrtA catalysis is facilitated by the formation of a substrate-stabilized oxyanion hole that may be a common feature in sortase enzymes.

A unique feature of the ^{Ba}SrtA-LPAT* complex is the presence of an N-terminal appendage that directly interacts with the bound peptide. The N-terminal appendage contacts the active site histidine residue and is poised to hydrogen bond to the backbone of the bound signal via the side chain of Ser^{59}. The appendage spans residues Asp^{57} to Val^{79} and contains helix H1. In the structure of the apo-form of the enzyme, the portion preceding helix H1 packs against the imidazole ring of His^{126} via contacts from the side chains of Ile^{61} and Pro^{64}. These interactions, along with contacts from Leu^{104} located in helix H2, shield the histidine side chain from the solvent (Fig. 5*B*). In the ^{Ba}SrtA-LPAT* complex, these interactions are largely preserved, except for contacts between His^{126} and Ile^{61} that are disrupted because the backbone of Ile^{61} and residues that precede it in the primary sequence are slightly displaced (Fig. 5*B*). This movement positions the side chain of Ser^{59} near the bound signal, potentiating hydrogen bonding interactions. The NMR relaxation data indicate that in both apo- and signal-bound forms of ^{Ba}SrtA the entire N-terminal appendage toggles between two distinct conformers, a closed conformation in which it contacts the catalytic core, and an open conformation in which residues including helix H1 of the appendage are detached from the body of the protein and become structurally disordered. The presence of the equilibrium is supported by the S^2 values of residues in the appendage, because in both the free and substrate-bound forms of the enzyme they exhibit small magnitudes (Fig. 3*D*). Detachment of the appendage presumably occurs on nanosecond or shorter time scales, because we were unable to detect significant R_{ex} values. Moreover, as the S^2 values progressively become smaller toward the N terminus of the protein the appendage presumably unlatches in a "peeling" motion. As compared with the full-length protein, the construct studied here by NMR is N terminally truncated (it is missing residues 1–56). It is therefore possible that on the cell surface these missing residues could also influence the structure of the N-terminal appendage and/or substrate access to the active site.

Interestingly, binding of the sorting signal may slightly destabilize latching of the N-terminal appendage to the core of enzyme, because the S^2 values of residues preceding helix H1 in the primary sequence positioned near the active site (Ile^{61}, Leu^{66}, and Ala^{67}) become smaller when the sorting signal binds to the enzyme (Fig. 5*C*). Three lines of evidence further support this assertion. First, a comparison of the NOESY spectra of the apo- and complexed forms of the protein reveals that substrate binding causes a 3-fold drop in intensity in the NOE cross-peaks that occur between residues located in the N-terminal appendage and the rest of the protein. Second, an analysis of the random coil index (RCI), a method to measure protein flexibility by comparing backbone chemical shifts to reference random coil shifts (70, 71), shows that residues in the N-terminal appendage have slightly higher RCI values when the LPAT* substrate analog is bound (Fig. 5*D*). Although the change in RCI is small, they occur in regions flanking helix H1 suggesting that when LPAT* binds there is an increased likelihood that the entire N-terminal appendage detaches from the protein. Last, a comparison of the structures of the apo- and complexed forms of the protein reveals that the substrate disrupts interactions between the side chains of Ile^{61} in the appendage and His^{126} in the active site, which presumably destabilize the closed form of the appendage. The biological significance of the destabilizing effects of signal binding on the attachment of the appendage is unclear, because the appendage is dynamic in both the free and bound states, and because the destabilizing effects are small.

Transient closure of the appendage over the sorting signal retards nucleophile access to the thioacyl reaction intermediate *in vitro*. On the cell surface, the first step in protein anchoring involves the formation of an enzyme-protein intermediate in which the threonine in the sorting signal of the protein substrate is connected to Cys^{187} via a thioacyl bond. This intermediate is then nucleophilically attacked by lipid II to form the protein-lipid II linked product of the sortase-catalyzed reaction. Our kinetics data probes the first steps of catalysis and monitors the rate at which the thioacyl bond is hydrolyzed by a water molecule that functions as a surrogate for lipid II (Table 2). Previously reported enzyme kinetic studies of the ^{Sa}SrtA enzyme have shown that nucleophilic attack by the water molecule is rate-limiting in the hydrolytic reaction (14, 15). Therefore, our observation that k_{cat} increases when a portion of the N-terminal appendage is removed suggests that its presence hinders nucleophile attack of the thioacyl bond. This notion is compatible with the increased k_{cat} of the I61A mutant as this alteration presumably disrupts contacts that stabilize positioning of the appendage over the active site. Importantly, the time scale of latching and unlatching of the appendage over the bound sorting signal is significantly shorter than the rate-limited hydrolysis step. Thus, in the isolated enzyme studied here, the N-terminal appendage repeatedly latches and unlatches over the thioacyl-linked sorting signal to hinder, but not completely prevent nucleophile access to the substrate.

The results of computational docking and whole cell display studies suggest that on the cell surface the N-terminal appendage may modulate lipid II access to the thioacyl intermediate. How sortases recognize lipid II remains unknown. To investigate the mechanism of binding we used the program FTSite to predict the binding site for *meso*-DAP, the amino group con-

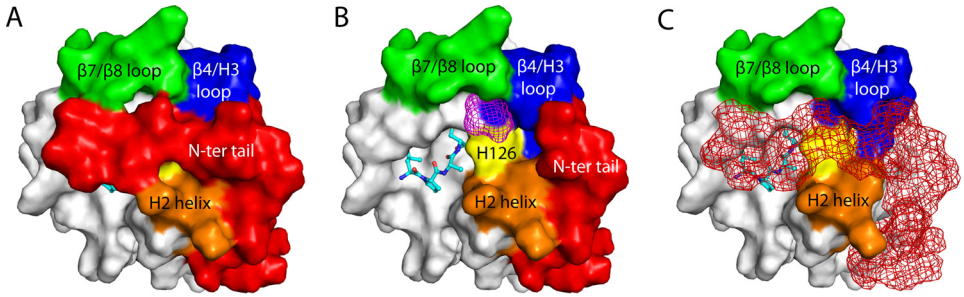

FIGURE 7. **The N-terminal appendage masks a potential binding site for lipid II.** The program FTSite was used to predict the binding site for DAP, the amino group containing moiety in the *B. anthracis* lipid II molecule that is joined to the sorting signal by sortase. The panels show solvent accessible surface representations of ^{Ba}SrtA-LPAT* (*A*) and ^{Ba}SrtA-LPAT* (*B*) in which residues Asp^{57}-Pro^{64} of the N-terminal appendage is removed. Only when residues Asp^{57}-Pro^{64} are removed is a potential binding site located near the active site observed (*magenta colored mesh*). In the figure, the N-terminal appendage, H2 helix, β4/H3 loop, β7/β8 loop, and active site His^{126} are colored *red*, *orange*, *blue*, *green*, and *yellow*, respectively. The substrate analog LPAT* is shown in stick format. *C*, as in *panel A*, but the N-terminal appendage is displayed as a *mesh* object.

taining moiety in the *B. anthracis* lipid II molecule that is joined to the sorting signal by sortase (72, 73). Two binding calculations were performed, one using the intact ^{Ba}SrtA-LPAT* complex, and a second in which the coordinates of the N-terminal appendage are removed. Only when a portion of the appendage is removed from ^{Ba}SrtA does FTSite predict the existence of a binding site for DAP that is located near the active site (compare Fig. 7, *A* and *B*). This site is located adjacent to His^{126}, and the β7/β8 and β4/H3 loops. Attractively, the site is near the electrophilic carbonyl carbon atom in the thioacyl bond, which could be accessed by the nucleophile with only minor rearrangements in the active site. Interestingly, only a few residues in the N-appendage (residues Asp^{57}-Pro^{64}) need to be displaced from the enzyme to unmask the DAP binding site such that helix H1 in the appendage could in principle remain attached during the transpeptidation reaction. The notion that residues Asp^{57}-Pro^{64} in the N-terminal appendage modulate substrate access is consistent with our whole cell studies, which revealed that S59G and I61A mutations in this segment of the appendage reduced display by ~50 and 40% as compared with the wild-type enzyme, respectively (Fig. 4*B*).

Similar to ^{Ba}SrtA, many class C enzymes that polymerize pili contain an N-terminal appendage that interacts with the active site. This appendage, called a "lid," is structurally distinct from the ^{Ba}SrtA appendage, and it approaches the active site from a different direction. Moreover, unlike the appendage in ^{Ba}SrtA, the lid more fully occludes the sorting signal binding site (74). When ^{Ba}SrtA is located in its natural context on the extracellular membrane, it is conceivable that its N-terminal appendage forms more extensive interactions with the body of the enzyme similar to the lid structure, which could cause it to fully occlude the binding site for the sorting signal. In this scenario, the N-terminal appendage might have a function similar to the lid, holding the sortase in an inactive state until factors on the cell surface detach it to promote sorting signal binding. Our modeling and biochemical studies also suggest that closure of the N terminus over the bound sorting signal hinders nucleophile access to the thioacyl bond that joins sortase to its protein substrate during the anchoring reaction. Thus, on the cell surface, the appendage may prevent unproductive hydrolysis of the thioacyl-linked enzyme-protein intermediate by masking the thioacyl bond from the solvent until lipid II, or other factors become available to complete the transpeptidation reaction. A deeper understanding of how sortase enzymes are regulated and the mechanism of catalysis will require structure determination of additional reaction intermediates that contain the substrate nucleophile, as well as a systematic investigation of how the enzyme operates on the cell surface.

Author Contributions—R. T. C., M. E. J., and A. W. M. designed and coordinated the study. A. H. C. and R. T. C. wrote the paper. A. H. C. purified the proteins, determined the NMR structure, and performed NMR dynamics, molecular dynamics and kinetics experiments. S. W. Y. synthesized boc-LPAT*. A. L. T. performed the *B. anthracis* cell experiments. All authors reviewed the results and approved the final version of the manuscript.

Acknowledgment—We thank Dr. Olaf Schneewind for kindly providing cells and plasmids for our in vivo experiments.

References

1. Mock, M., and Fouet, A. (2001) Anthrax. *Annu. Rev. Microbiol.* **55,** 647–671
2. Holty, J. E., Bravata, D. M., Liu, H., Olshen, R. A., McDonald, K. M., and Owens, D. K. (2006) Systematic review: a century of inhalational anthrax cases from 1900 to 2005. *Ann. Intern. Med.* **144,** 270–280
3. Zink, S. D., and Burns, D. L. (2005) Importance of srtA and srtB for growth of *Bacillus anthracis* in macrophages. *Infect. Immun.* **73,** 5222–5228
4. Cascioferro, S., Totsika, M., and Schillaci, D. (2014) Sortase A: an ideal target for anti-virulence drug development. *Microb. Pathog.* **77,** 105–112
5. Schneewind, O., and Missiakas, D. (2014) Sec-secretion and sortase-mediated anchoring of proteins in Gram-positive bacteria. *Biochim. Biophys. Acta* **1843,** 1687–1697
6. Spirig, T., Weiner, E. M., and Clubb, R. T. (2011) Sortase enzymes in Gram-positive bacteria. *Mol. Microbiol.* **82,** 1044–1059
7. Clancy, K. W., Melvin, J. A., and McCafferty, D. G. (2010) Sortase transpeptidases: insights into mechanism, substrate specificity, and inhibition. *Biopolymers* **94,** 385–396
8. Hendrickx, A. P., Budzik, J. M., Oh, S. Y., and Schneewind, O. (2011) Architects at the bacterial surface: sortases and the assembly of pili with isopeptide bonds. *Nat. Rev. Microbiol.* **9,** 166–176
9. Maresso, A. W., and Schneewind, O. (2008) Sortase as a target of anti-infective therapy. *Pharmacol. Rev.* **60,** 128–141
10. Scott, J. R., and Zähner, D. (2006) Pili with strong attachments: Gram-positive bacteria do it differently. *Mol. Microbiol.* **62,** 320–330
11. Suree, N., Jung, M. E., and Clubb, R. T. (2007) Recent advances towards new anti-infective agents that inhibit cell surface protein anchoring in *Staphylococcus aureus* and other Gram-positive pathogens. *Mini. Rev. Med. Chem.* **7,** 991–1000
12. Finn, R. D., Mistry, J., Tate, J., Coggill, P., Heger, A., Pollington, J. E., Gavin,

O. L., Gunasekaran, P., Ceric, G., Forslund, K., Holm, L., Sonnhammer, E. L., Eddy, S. R., and Bateman, A. (2010) The Pfam protein families database. *Nucleic Acids Res.* **38,** D211–222
13. Schneewind, O., Model, P., and Fischetti, V. A. (1992) Sorting of protein A to the staphylococcal cell wall. *Cell* **70,** 267–281
14. Huang, X., Aulabaugh, A., Ding, W., Kapoor, B., Alksne, L., Tabei, K., and Ellestad, G. (2003) Kinetic mechanism of *Staphylococcus aureus* sortase SrtA. *Biochemistry* **42,** 11307–11315
15. Frankel, B. A., Kruger, R. G., Robinson, D. E., Kelleher, N. L., and McCafferty, D. G. (2005) *Staphylococcus aureus* sortase transpeptidase SrtA: insight into the kinetic mechanism and evidence for a reverse protonation catalytic mechanism. *Biochemistry* **44,** 11188–11200
16. Ton-That, H., and Schneewind, O. (2004) Assembly of pili in Gram-positive bacteria. *Trends Microbiol.* **12,** 228–234
17. Comfort, D., and Clubb, R. T. (2004) A comparative genome analysis identifies distinct sorting pathways in Gram-positive bacteria. *Infect. Immun.* **72,** 2710–2722
18. Dramsi, S., Trieu-Cuot, P., and Bierne, H. (2005) Sorting sortases: a nomenclature proposal for the various sortases of Gram-positive bacteria. *Res. Microbiol.* **156,** 289–297
19. Aucher, W., Davison, S., and Fouet, A. (2011) Characterization of the sortase repertoire in *Bacillus anthracis*. *PLoS ONE* **6,** e27411
20. Gaspar, A. H., Marraffini, L. A., Glass, E. M., Debord, K. L., Ton-That, H., and Schneewind, O. (2005) *Bacillus anthracis* sortase A (SrtA) anchors LP*X*TG motif-containing surface proteins to the cell wall envelope. *J. Bacteriol.* **187,** 4646–4655
21. Maresso, A. W., Chapa, T. J., and Schneewind, O. (2006) Surface protein IsdC and Sortase B are required for heme-iron scavenging of *Bacillus anthracis*. *J. Bacteriol.* **188,** 8145–8152
22. Marraffini, L. A., and Schneewind, O. (2007) Sortase C-mediated anchoring of BasI to the cell wall envelope of *Bacillus anthracis*. *J. Bacteriol.* **189,** 6425–6436
23. Weiner, E. M., Robson, S., Marohn, M., and Clubb, R. T. (2010) The Sortase A enzyme that attaches proteins to the cell wall of *Bacillus anthracis* contains an unusual active site architecture. *J. Biol. Chem.* **285,** 23433–23443
24. Delaglio, F., Grzesiek, S., Vuister, G. W., Zhu, G., Pfeifer, J., and Bax, A. (1995) NMRPipe: a multidimensional spectral processing system based on UNIX pipes. *J. Biomol. NMR* **6,** 277–293
25. Garrett, D. S., Powers, R., Gronenborn, A. M., and Clore, G. M. (1991) A common sense approach to peak picking in two-, three-, and four-dimensional spectra using automatic computer analysis of contour diagrams. *J. Magn. Reson.* **95,** 214–220
26. Keller, R. (2004) *The Computer Aided Resonance Assignment Tutorial*, CATINA Verlag, Goldau, Switzerland
27. Cavanagh, J., Fairbrother, W. J., Palmer, A. G., and Skelton, N. J. (2006) *Protein NMR spectroscopy*, 2nd Ed., Elsevier Science and Technology, San Diego, CA
28. Teng, Q. (2005) *Structural Biology: Practical NMR Applications*, Springer Verlag, New York
29. Iwahara, J., Wojciak, J. M., and Clubb, R. T. (2001) Improved NMR spectra of a protein-DNA complex through rational mutagenesis and the application of a sensitivity optimized isotope-filtered NOESY experiment. *J. Biomol. NMR* **19,** 231–241
30. Zwahlen, C., Legault, P., Vincent, S. J. F., Greenblatt, J., Konrat, R., and Kay, L. E. (1997) Methods for measurement of intermolecular NOEs by multinuclear NMR spectroscopy: application to a bacteriophage λ N-peptide/boxB RNA complex. *J. Am. Chem. Soc.* **119,** 6711–6721
31. Shen, Y., Delaglio, F., Cornilescu, G., and Bax, A. (2009) TALOS+: a hybrid method for predicting protein backbone torsion angles from NMR chemical shifts. *J. Biomol. NMR* **44,** 213–223
32. Vuister, G. W., and Bax, A. (1993) Quantitative J correlation: a new approach for measuring homonuclear three-bond J(HNH.α) coupling constants in ^{15}N-enriched proteins. *J. Am. Chem. Soc.* **115,** 7772–7777
33. Gagné, S. M., Tsuda, S., Li, M. X., Chandra, M., Smillie, L. B., and Sykes, B. D. (1994) Quantification of the calcium-induced secondary structural changes in the regulatory domain of troponin-C. *Protein Sci.* **3,** 1961–1974
34. Clore, G. M., Bax, A., and Gronenborn, A. M. (1991) Stereospecific assignment of β-methylene protons in larger proteins using 3D ^{15}N-separated Hartmann-Hahn and ^{13}C-separated rotating frame Overhauser spectroscopy. *J. Biomol. NMR* **1,** 13–22
35. Powers, R., Garrett, D. S., March, C. J., Frieden, E. A., Gronenborn, A. M., and Clore, G. M. (1993) The high-resolution, three-dimensional solution structure of human interleukin-4 determined by multidimensional heteronuclear magnetic resonance spectroscopy. *Biochemistry* **32,** 6744–6762
36. Herrmann, T., Güntert, P., and Wüthrich, K. (2002) Protein NMR structure determination with automated NOE-identification in the NOESY spectra using the new software ATNOS. *J. Biomol. NMR* **24,** 171–189
37. Herrmann, T., Güntert, P., and Wüthrich, K. (2002) Protein NMR structure determination with automated NOE assignment using the new software CANDID and the torsion angle dynamics algorithm DYANA. *J. Mol. Biol.* **319,** 209–227
38. Schwieters, C. D., Kuszewski, J. J., Tjandra, N., and Clore, G. M. (2003) The Xplor-NIH NMR molecular structure determination package. *J. Magn. Reson.* **160,** 65–73
39. Grishaev, A., and Bax, A. (2004) An empirical backbone-backbone hydrogen-bonding potential in proteins and its applications to NMR structure refinement and validation. *J. Am. Chem. Soc.* **126,** 7281–7292
40. Ruckert, M., and Otting, G. (2000) Alignment of biological macromolecules in novel nonionic liquid crystalline media for NMR experiments. *J. Am. Chem. Soc.* **122,** 7793–7797
41. Ottiger, M., Delaglio, F., and Bax, A. (1998) Measurement of J and dipolar couplings from simplified two-dimensional NMR spectra. *J. Magn. Reson.* **131,** 373–378
42. Bax, A., Kontaxis, G., and Tjandra, N. (2001) Dipolar couplings in macromolecular structure determination. *Methods Enzymol.* **339,** 127–174
43. Dosset, P., Hus, J. C., Marion, D., and Blackledge, M. (2001) A novel interactive tool for rigid-body modeling of multi-domain macromolecules using residual dipolar couplings. *J. Biomol. NMR* **20,** 223–231
44. Koradi, R., Billeter, M., and Wuthrich, K. (1996) MOLMOL: a program for display and analysis of macromolecular structures. *J. Mol. Graph.* **14,** 51–55, 29–32
45. DeLano, W. L. (2006) *The PyMOL Molecular Graphics System*, DeLano Scientific, LLC, Palo Alto, CA
46. Goddard, T. D., and Kneller, D. G. (2006) *SPARKY 3*, University of California, San Francisco, CA
47. Naik, M. T., Suree, N., Ilangovan, U., Liew, C. K., Thieu, W., Campbell, D. O., Clemens, J. J., Jung, M. E., and Clubb, R. T. (2006) *Staphylococcus aureus* Sortase A transpeptidase: calcium promotes sorting signal binding by altering the mobility and structure of an active site loop. *J. Biol. Chem.* **281,** 1817–1826
48. Brüschweiler, R., Liao, X., and Wright, P. E. (1995) Long-range motional restrictions in a multidomain zinc-finger protein from anisotropic tumbling. *Science* **268,** 886–889
49. Lee, L. K., Rance, M., Chazin, W. J., and Palmer, A. G., 3rd. (1997) Rotational diffusion anisotropy of proteins from simultaneous analysis of ^{15}N and ^{13}Cα nuclear spin relaxation. *J. Biomol. NMR* **9,** 287–298
50. Lipari, G., and Szabo, A. (1982) Model-free approach to the interpretation of nuclear magnetic resonance relaxation in macromolecules: 1. theory and range of validity. *J. Am. Chem. Soc.* **104,** 4546–4559
51. Lipari, G., and Szabo, A. (1982) Model-free approach to the interpretation of nuclear magnetic resonance relaxation in macromolecules: 2. analysis of experimental results. *J. Am. Chem. Soc.* **104,** 4559–4570
52. Cole, R., and Loria, J. P. (2003) FAST-Modelfree: a program for rapid automated analysis of solution NMR spin-relaxation data. *J. Biomol. NMR* **26,** 203–213
53. Mandel, A. M., Akke, M., and Palmer, A. G., 3rd (1995) Backbone dynamics of *Escherichia coli* ribonuclease HI: correlations with structure and function in an active enzyme. *J. Mol. Biol.* **246,** 144–163
54. Jacobitz, A. W., Wereszczynski, J., Yi, S. W., Amer, B. R., Huang, G. L., Nguyen, A. V., Sawaya, M. R., Jung, M. E., McCammon, J. A., and Clubb, R. T. (2014) Structural and computational studies of the *Staphylococcus aureus* sortase B-substrate complex reveal a substrate-stabilized oxyanion hole. *J. Biol. Chem.* **289,** 8891–8902
55. Case, D. A., Darden, T. A., Cheatham, T. E., Simmerling, C. L., Wang, J.,

Duke, R. E., Luo, R., Walker, R. C., Zhang, W., Merz, K. M., Roberts, B., Hayik, S., Roitberg, A., Seabra, G., Swails, J., Goetz, A. W., Kolossvary, I., Wong, K. F., Paesani, F., Vanicek, J., Wolf, R. M., Liu, J., Wu, X., Brozell, S. R., Steinbrecher, T., Gohlke, H., Cai, Q., Ye, X., Wang, J., Hsieh, M. J., Cui, G., Roe, D. R., Mathews, D. H., Seetin, M. G., Salomon-Ferrer, R., Sagui, C., Babin, V., Luchko, T., Gusarov, S., Kovalenko, A., and Kollman, P. A. (2012) *AMBER 12*, University of California, San Francisco, CA

56. Phillips, J. C., Braun, R., Wang, W., Gumbart, J., Tajkhorshid, E., Villa, E., Chipot, C., Skeel, R. D., Kalé, L., and Schulten, K. (2005) Scalable molecular dynamics with NAMD. *J. Comput. Chem.* **26,** 1781–1802
57. Suree, N., Yi, S. W., Thieu, W., Marohn, M., Damoiseaux, R., Chan, A., Jung, M. E., and Clubb, R. T. (2009) Discovery and structure-activity relationship analysis of *Staphylococcus aureus* sortase A inhibitors. *Bioorg. Med. Chem.* **17,** 7174–7185
58. Jung, M. E., Clemens, J. J., Suree, N., Liew, C. K., Pilpa, R., Campbell, D. O., and Clubb, R. T. (2005) Synthesis of (2*R*,3*S*)3-amino-4-mercapto-2-butanol, a threonine analogue for covalent inhibition of sortases. *Bioorg. Med. Chem. Lett.* **15,** 5076–5079
59. Jung, M. E., and Yi, S. W. (2012) Synthesis of threo-β-aminoalcohols from aminoaldehydes via chelation-controlled additions: total synthesis of L-threo-sphingosine and safingol. *Tetrahedron Lett.* **53,** 4216–4220
60. Liew, C. K., Smith, B. T., Pilpa, R., Suree, N., Ilangovan, U., Connolly, K. M., Jung, M. E., and Clubb, R. T. (2004) Localization and mutagenesis of the sorting signal binding site on sortase A from *Staphylococcus aureus*. *FEBS Lett.* **571,** 221–226
61. Schechter, I., and Berger, A. (1967) On the size of the active site in proteases: I. papain. *Biochem. Biophys. Res. Commun.* **27,** 157–162
62. Aucher, W., Davison, S., and Fouet, A. (2011) Characterization of the sortase repertoire in *Bacillus anthracis*. *PLoS ONE* **6,** e27411
63. Palmer, A. G., 3rd, Kroenke, C. D., and Loria, J. P. (2001) Nuclear magnetic resonance methods for quantifying microsecond-to-millisecond motions in biological macromolecules. *Methods Enzymol.* **339,** 204–238
64. Tollinger, M., Skrynnikov, N. R., Mulder, F. A., Forman-Kay, J. D., and Kay, L. E. (2001) Slow dynamics in folded and unfolded states of an SH3 domain. *J. Am. Chem. Soc.* **123,** 11341–11352
65. Kleckner, I. R., and Foster, M. P. (2011) An introduction to NMR-based approaches for measuring protein dynamics. *Biochim. Biophys. Acta* **1814,** 942–968
66. Loria, J. P., Berlow, R. B., and Watt, E. D. (2008) Characterization of enzyme motions by solution NMR relaxation dispersion. *Acc. Chem. Res.* **41,** 214–221
67. Schneewind, O., and Missiakas, D. M. (2012) Protein secretion and surface display in Gram-positive bacteria. *Philos. Trans. R. Soc. Lond. B Biol. Sci.* **367,** 1123–1139
68. Suree, N., Liew, C. K., Villareal, V. A., Thieu, W., Fadeev, E. A., Clemens, J. J., Jung, M. E., and Clubb, R. T. (2009) The structure of the *Staphylococcus aureus* sortase-substrate complex reveals how the universally conserved LPXTG sorting signal is recognized. *J. Biol. Chem.* **284,** 24465–24477
69. Zong, Y., Mazmanian, S. K., Schneewind, O., and Narayana, S. V. (2004) The structure of sortase B, a cysteine transpeptidase that tethers surface protein to the *Staphylococcus aureus* cell wall. *Structure* **12,** 105–112
70. Berjanskii, M. V., and Wishart, D. S. (2005) A simple method to predict protein flexibility using secondary chemical shifts. *J. Am. Chem. Soc.* **127,** 14970–14971
71. Berjanskii, M. V., and Wishart, D. S. (2008) Application of the random coil index to studying protein flexibility. *J. Biomol. NMR* **40,** 31–48
72. Ngan, C. H., Hall, D. R., Zerbe, B., Grove, L. E., Kozakov, D., and Vajda, S. (2012) FTSite: high accuracy detection of ligand binding sites on unbound protein structures. *Bioinformatics* **28,** 286–287
73. Brenke, R., Kozakov, D., Chuang, G. Y., Beglov, D., Hall, D., Landon, M. R., Mattos, C., and Vajda, S. (2009) Fragment-based identification of druggable "hot spots" of proteins using Fourier domain correlation techniques. *Bioinformatics* **25,** 621–627
74. Manzano, C., Contreras-Martel, C., El Mortaji, L., Izoré, T., Fenel, D., Vernet, T., Schoehn, G., Di Guilmi, A. M., and Dessen, A. (2008) Sortase-mediated pilus fiber biogenesis in *Streptococcus pneumoniae*. *Structure* **16,** 1838–1848